# Nonlinear spectral features of the relativistic interaction between electron and ultrashort laser pulse

Ziqiang Shao,[1] Quanli Dong,[1,2,*] Hao Teng,[3] Zhe Li,[1] Dongning Yue,[1] Qingcao Liu,[1] Zhiyi Wei,[3] and Jie Zhang[2,3,4]

[1]*School of Physics, Harbin Institute of Technology, Harbin 150001, China*

[2]*Collaborative Innovation Center of IFSA (CICIFSA), Shanghai Jiao Tong University, Shanghai 200240, China*

[3]*Beijing National Laboratory for Condensed Matter Physics, Institute of Physics, Chinese Academy of Sciences, Beijing 100190, China*

[4]*Key Laboratory for Laser Plasmas and School of Physics and Astronomy, Shanghai Jiao Tong University, Shanghai 200240, China*

(Received 17 November 2022; revised 12 April 2023; accepted 24 April 2023; published 12 May 2023)

Features of the radiation spectra are investigated with the quantum electrodynamic theory for the nonlinear scattering interaction between relativistic electron and few-cycle linearly polarized laser pulse. The angle between the moving direction of the electron and that of the laser pulse affects the scattered radiation characteristics. When the electron has a head-on collision with the laser pulse having a carrier envelope phase as zero, the angular distribution of the scattered radiation spectrum is symmetrical with respect to the laser pulse propagation direction. Such a symmetry disappears when the electron collides with the laser obliquely and the direction of most of the radiation energy shifts at an acute angle towards the electron direction. The CEP has significant effects on the spectral angular distribution. The CEP influence is determined by the exertion of the electromagnetic field on the motion of the electron, whose trajectory overlap in phase space leads to the interference between scattered radiation in different intervals of the interaction process. The supercontinuum radiation could be produced under certain CEPs. An external electrostatic field applied as the environment for the laser-electron interaction is another important factor affecting the scattered radiation features by modulating the harmonic components and their angular distribution. This study may help the analysis of the spectral data from relativistic laser-solid target experiments.

DOI: 10.1103/PhysRevA.107.053109

## I. INTRODUCTION

The process of strong-field quantum electrodynamics can be studied by investigating ultrarelativistic electron collisions with relativistically intense laser pulses, such as nonlinear scattering (NCS) [1–4], nonlinear Breit-Wheeler pair production [5–12], electron-positron annihilation [13], etc. The nonlinear quantum effects can be described by the dimensionless parameter $\chi = (k_L p)\xi_L/|e|E_c$, where $\xi_L = |e|E_L/m\omega_L$ is the classical intensity parameter with the electron mass $m$ and charge $e < 0$, $E_c = m^2/|e|$ is the Schwinger critical field of $\sim 1.3 \times 10^{16}$ V/m [11,12,14], and $k_L p$ is the product of the laser four-wave-vector $k_L^\mu$ and the electrons four-momentum $p^\mu$ under Minkowski metric, where Greek indices $\mu$ run over 0, 1, 2, 3. Natural units with $\hbar = c = 1$ are utilized above and will be used throughout the whole context unless otherwise specified.

The leading-order process of NCS is the nonlinear single Compton scattering (NSCS), in which an electron scatters multilaser photons into one higher-energy photon. The process in a classical manner is usually named as the nonlinear Thomson scattering, which needs to be corrected as $\chi \to 1$ when the quantum effects become important [15–18]. For an electron interacting with a monochromatic plane wave, the radiation frequency spectrum is discrete [19]. When the interacting electromagnetic field is a pulsed plane wave, the harmonic peaks of the nonlinear Compton spectrum become broader and present numerous subpeaks [18,20–22]. For an electron interacting with a one-cycle laser pulse, the multiphoton peaks are significantly broadened [23]. The electric and magnetic field distribution in the laser temporal envelope of this kind of laser pulse, which is characterized by the carrier envelope phase (CEP), determines the whole process of the interaction with electrons. In the interaction, the angular distribution of the Compton radiation energy obtained by integrating within the plane perpendicular to the laser polarization becomes asymmetrical, which is the consequence of asymmetry of the laser vector potential with respect to the change of the electric component direction [24]. Mackenroth and co-authors used the angular distribution of the radiation in multiphoton Compton scattering to determine the CEP of the ultrarelativistic few-cycle laser pulse [25]. The scattering direction of the high-energy photons is closely related to the interacting laser intensity, the increment of which from the nonrelativistic to relativistic regime changes the dominant scattering direction from that perpendicular to the laser polarization to the parallel direction [26].

The relativistic interaction between electrons and electromagnetic fields is governed by the second-order Dirac equation, which describes electrons in the so-called Volkov state [27,28]. When the initial electron is in a superposition of states, the different momentum components do not interfere with each other, and the net effects of this on the angular-resolved emission spectrum are the peak broadening

*qldong@aphy.iphy.ac.cn

 

and smoothing, which dominates over the effects of the uncertainty in laser frequency [29]. For an electron inside a laser propagating in plasmas with refractive index $n < 1$ [30–33] or in a rotating electric field [34,35], the Dirac equation has no general solution since the dispersion relation $(k_L)^2 \neq 0$, indicating that the second-order Dirac equation cannot be reduced to the first-order one. The multiple-scale perturbation theory was used to resolve the equation for electron states when the laser travels in a plasma. But the influence of plasma on the electron was ignored in the case with cold and collisionless plasma [30].

The above-mentioned works mainly focus on head-on collision between energetic electrons with $\gamma_e \gg 1$ and ultraintense laser pulses with $\xi_L \gg 1$. The main presented results are the angular distribution of radiated energy or the spectra at a fixed observation direction along the initial electron direction. The NSCS in the case of laser-electron oblique collision inside an electrostatic field has not yet been reported.

In this paper, we report details of the angular-distributed spectra of the scattered radiation from interactions between laser pulses at moderate intensity ($\xi_L = 2$) and electrons with not-so-high energies ($\gamma_e = 2$) when they head-on or obliquely collide in an electrostatic field. The subject is closely related to present studies about attosecond laser pulse generation in laser-solid target interaction through the coherent synchrotron emission (CSE) mechanism, in which the laser-electron collision has an angle and the electron also feels the electrostatic field resulted from the charge separation [36–39]. Section II presents characteristics of the angular distribution of the radiation spectra when the laser pulse collides with electrons head on and obliquely. The results in the case of head-on collision reproduce previous achievements of the radiation energy angular distribution and the spectra when we take the frequency integration and the angular integration, respectively. Comparisons between results from classical theory and Quantum electrodynamics (QED) are also given in this section. Section III presents results from laser-electron collisions in an electrostatic field.

## II. LASER-ELECTRON HEAD-ON AND OBLIQUE COLLISION

### A. Basic equations

The laser pulse propagating along the $z$ axis is described as a plane wave linearly polarized along the $y$ axis. Its classical four-vector potential is $A_L^\mu = \psi_L(\phi_L)a_L^\mu = [0, 0, -\psi_L(\phi_L)m\xi_L/e, 0]$, where $\psi_L(\phi_L) = \sin^4(\phi_L/2N)\sin(\phi_L + \phi_{cep})$ in $\phi_L \in [0, 2\pi N]$ and zero for other $\phi_L$, with $\phi_{cep}$ as the carrier envelope phase (CEP), $N$ as the number of oscillation cycles, and $\phi_L = \omega_L(t - z)$ as the laser phase. In the following, we will take $N = 2$, $\omega_L = 1.55$ eV. The fast Fourier transform on the laser electric field profile gives the central frequency of the electric field spectrum as about 1.94 eV. An initial electron with an energy of 1 MeV is assumed to propagate at $\delta = 0$ or $\theta = 135^\circ$ with respect to the negative $z$ direction, as shown in Figs. 1(a) and 1(b), which are situations of laser-electron head-on and oblique collision, respectively.

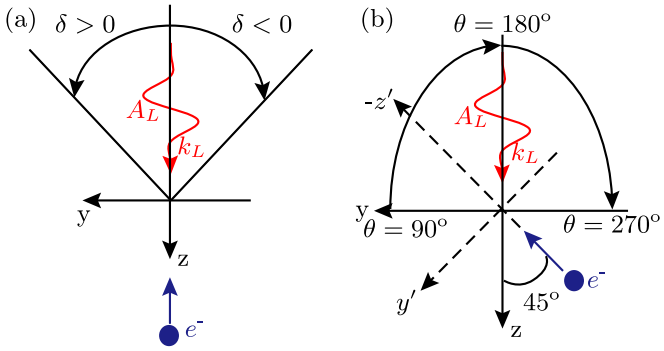


FIG. 1. Schematic illustration of laser-electron interaction scene for (a) head-on collision and (b) oblique collision.

Within the Furry picture [40], the interaction between the electron and the strong laser field is taken into account exactly, but the interaction between the electron and emitted photons is treated as a perturbation. The contribution of the scattering process to the whole spectra decreases as $\alpha^n$, where $\alpha = e^2 \approx 1/137$ is the fine-structure constant under additional Gaussian units and $n$ is the number of emitted photons [23,41]. Thus, we only consider NSCS and neglect the high-order processes. The scattering amplitude of NSCS is written as [42]

$$S_{fi} = -ie \int_{-\infty}^{+\infty} \overline{\psi}_{p'} \not{A}^*_{k'} \psi_p \, d^4x, \tag{1}$$

where $\psi_p$ with four-momentum $p^\mu$ is the initial electron's Volkov states [27], $\overline{\psi}_{p'}$ is the Dirac conjugate of the final Volkov states, and $A^\mu_{k'}$ with four-wave-vector $k'^\mu$ is the emitted photon's wave function. Throughout the paper, the Feynman slash notation is used.

For the convenience to calculate the integral, the light-cone coordinates with the notations $q^- = q_0 - q_z$, $q^+ = q_0 + q_z$ and $q^\perp = (q_x, q_y)$ for any four-vector $q^\mu$ are introduced. While the integrals of $x$, $y$, and $t - z$ lead to three delta functions indicating energy momentum conservation relations, the remaining integral on $\phi_L = k_L x$ contains

$$f_n = \int_{-\infty}^{+\infty} \psi_L^n(\phi_L) e^{i\{\zeta\phi_L + \int_0^{\phi_L}[\alpha\psi(\phi'_L) + \beta\psi^2(\phi'_L)]d\phi'_L\}} d\phi_L,$$
$$n = \{0, 1, 2\}, \tag{2}$$

with

$$\zeta = \frac{p'^+ + k'^+ - p^+}{2\omega_L},$$
$$\alpha = \frac{e(ap')}{kp'} - \frac{e(ap)}{kp}, \ \beta = \frac{e^2a^2}{2kp} - \frac{e^2a^2}{2kp'}. \tag{3}$$

Multiplying the squared modulus of the scattering amplitude by the number of states of the final particle in the phase space, the energy emission rate is obtained after averaging over initial electron spins and summing over the final electron spins and the emitted photon polarization states. Thus, in unit solid angle $\Omega$ and unit frequency interval $\omega'$, the emitted

photon energy spectrum can be written as

$$\frac{dE'}{d\Omega d\omega'} = \frac{e^2\omega'^2}{\omega_L^2 p^- p'^- (2\pi)^2}\Bigg[(pp' - 2m^2)|f_0|^2 + \left(\frac{-e^2a_L^2(k_Lp')}{2k_Lp} + \frac{-e^2a_L^2(k_Lp)}{2k_Lp'}\right)|f_1|^2 + e^2a_L^2\mathrm{Re}(f_0f_2^*) + \left(\frac{e[(a_Lp')(k_Lp) - (a_Lp)(k_Lp')]}{k_Lp'} + \frac{e[(a_Lp)(k_Lp') - (a_Lp')(k_Lp)]}{k_Lp}\right)\mathrm{Re}(f_0f_1^*)\Bigg]. \quad (4)$$

Here, the scalar product $a_Lp$ does not equal zero in the laser-electron oblique collision. For the laser-electron head-on collision, Eq. (4) reduces to Eq. (28) in Ref. [23].

### B. Results for head-on collision

Figure 2 shows the angular-distributed spectra for an electron head-on collision with a laser pulse of CEP = 0 and $\chi \sim 2.3 \times 10^{-5}$. The shape of the vector potential of the laser pulse exhibits symmetry with the change of the polarization vector direction $\epsilon_1 \to -\epsilon_1$ when CEP = 0, which causes the symmetry of the angular distribution with respect to $\delta = 0$ in Fig. 2.

In the direction of $\delta = 0$, the emitted photons around 11 eV, 33 eV, 55 eV *et al.* are harmonics with a certain frequency width resulted from the fact that the ultrashort laser pulse has a certain frequency width [18,23]. In the directions deviating from $\delta = 0$, for the $n$th-order harmonic, the relation between the radiating angle and frequency of the emitted photons shows a parabolic shape and the profile's opening angle decreases with the harmonic order $n$.

For the case of monochromatic laser field, the frequency of the $n$th harmonic can be written as [29,41]

$$\omega_n'[n'(\delta)] = \frac{n(kp)}{(q + nk)n'} = \frac{n(kp)}{\left(p + \frac{m^2\xi_L^2}{4(kp)}k\right)n' + n(kn')}, \quad (5)$$

where $n'(\delta) = [1, 0, \sin(\delta), -\cos(|\delta|)]$ is the observation direction, and $|\delta|$ is the angle deviation from the initial electron moving direction. $k = (\omega_0, 0, 0, \omega_0)$ is the four-wave-vector of the monochromatic plane wave and $q$ is the quasimomentum of electron.

For an electron with $\gamma_e \gg 1$, the radiation is mainly in a narrow cone along its velocity [25,26]. For the current case, the radiation distributes in a large angle range. For $\delta \neq 0$, $p_y \neq 0$ and $p_0$ and $p_z$ are always taken as their initial values. When taking $p_y = p_{y\max} = 1.55m$ for $\delta > 0$, $p_y = p_{y\min} = -1.55m$ for $\delta < 0$, $n = 1$, and $\omega_0$ equals the central frequency of the laser pulse of 1.94 eV, the relation between the radiation angle $\delta$ and the frequency $\omega'$ of the $n$th harmonic photons in Eq. (5) are shown as the red dashed lines in Fig. 2. In the $\delta = 0$ direction, the frequency in the red line is smaller than the central frequency of the first harmonic, since in the denominator of Eq. (5) the electron quasimomentum $q$ taken as that in the monochromatic wave case is larger than that in the current ultrashort pulse case [18]. In Eq. (5), $n(kn')$ can be neglected compared to its left item, and thus $\omega_n'$ is proportional to the $\omega_0$. The $|p_y|$ value taken in Eq. (5) controls the opening angle the plotted line relative to $\delta = 0$ direction. An increase in $|p_y|$ results in a decrease in the opening angle. When taking $\omega_0 = 2.35$ eV, $p_0 = 1.6m$, and $n = 1, 2, 3$, we plot black dashed lines in Fig. 2 and find that the analytical model coincides well with the numerical calculations.

The process of the NSCS takes places in the longitudinal length of the order of $\lambda_0/\xi_L$, which is $\lambda_0/2$ here, with $\lambda_0$ being the central wavelength of the laser pulse [41,43]. To understand the scattering process, the angular spectra in different half-cycles are shown in Fig. 3. The angular spectra radiated in the first laser half-cycle is calculated from Eq. (4) by integrating $\phi_L$ over $(0, \pi)$ in Eq. (2), and the angular spectra from

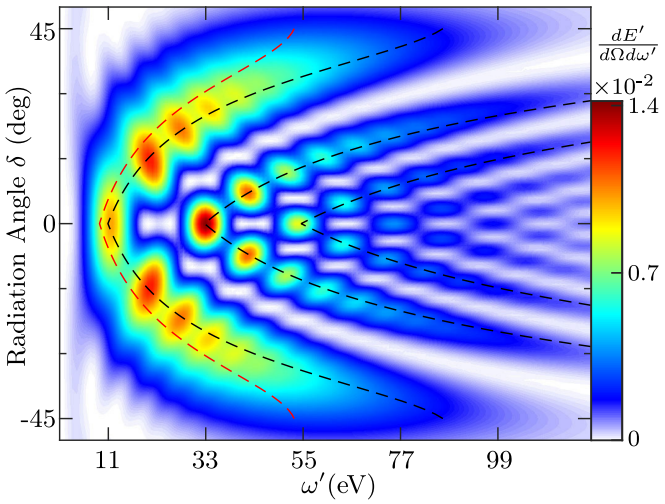


FIG. 2. Angular spectra in the laser polarization plane ($yoz$) for Laser-electron head-on collision. The parameters of the laser pulse are N = 2, CEP = 0, and $\xi_L = 2$, and the initial electron energy is 1 MeV. The dashed lines are plotted from Eq. (5).

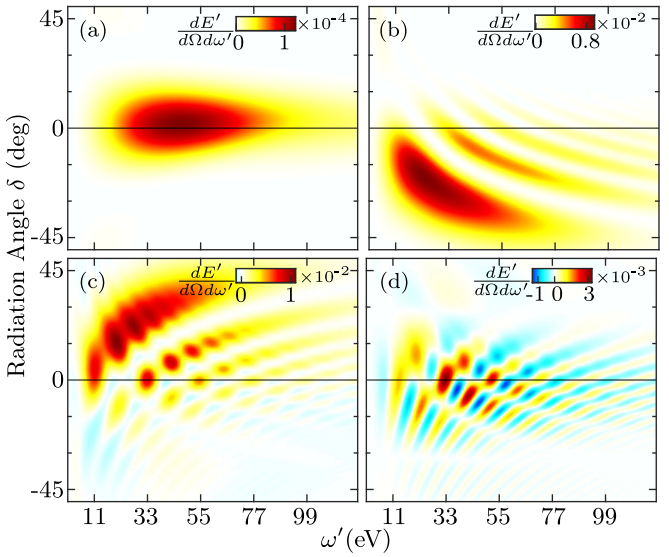


FIG. 3. (a)–(d) Angular spectra from four successive half-cycles for the case in Fig. 2.

the second half-cycle is obtained by subtracting the spectra during $0 < \phi_L < 1\pi$ from the spectra during $0 < \phi_L < 2\pi$. The angular spectra from the third and fourth half-cycle can be obtained through the same method. When CEP = 0, whether the emission locates above or below the line $\delta = 0$ is essentially determined by the direction of the vector potential. In the first half-cycle when laser intensity $\xi_L \ll 1$, the radiation is mainly focused in a cone angle of $\Delta\delta \sim 1/\gamma_e$. The largest part of the radiated energy of the whole spectra is emitted in the second and third lasers' half-cycles when the vector potential is large. But the radiations from the two half-cycles are distributed on the opposite sides of the line $\delta = 0$. For the radiation from the last half-cycle, the negative value of the radiated energy at some specific frequencies and the wider emission angle can be explained by taking consideration of dynamics of the electron.

The electron's motion features in the whole process are obtained by solving the relativistic motion equation [44,45]

$$\begin{aligned} \frac{dp_y}{dt} &= E_y + \beta_z B_x, \\ \frac{dp_z}{dt} &= -\beta_y B_x = \beta_y E_y, \\ \gamma_e^2 &= 1 + p_y^2 + p_z^2, \end{aligned} \tag{6}$$

where we take the dimensionless variables

$$\begin{aligned} (t, y, z) &= (\omega t, k_L y, k_L z), \\ (p_y, p_z) &= \left(\frac{p_y}{mc}, \frac{p_z}{mc}\right), \\ (E_y, B_x, A) &= \frac{(E_y, B_x, A)e}{mc\omega_L}. \end{aligned} \tag{7}$$

For the laser pulse, $B_x = -E_y$, $E_y(\phi_L) = -\omega_L A_L'(\phi_L)/c$, and $A_L(\phi_L) = -\xi_L \psi_L(\phi_L)/c\omega_L$, with $d\phi_L/dt = (1 - \beta_z)$, and $\beta = v/c$ is the electron velocity normalized to light velocity. Equation (6) gives $p_y$ and $p_z$ in the natural units as

$$\begin{aligned} p_y &= p_{y0} + \xi_L \psi_a(\phi_L), \\ p_z &= \frac{1 + p_y^2}{2C} - \frac{C}{2} = \frac{1 + [p_{y0} + \xi_L \psi_a(\phi_L)]^2}{2C} - \frac{C}{2}, \end{aligned} \tag{8}$$

where the constant $C = \gamma_{e0} - p_{z0}$, and $\gamma_{e0}$ and $p_{z0}$ are the initial relativistic factor and momentum in the $z$ direction, respectively. The instantaneous direction of the electron $\delta_e = \arctan(p_y/|p_z|)$.

The change tendency of $p_y$ is consistent with that of the vector potential shape function $\psi_a(\phi_L)$ and the change of $p_z$ as a function of $\phi_L$ is symmetrical, which results in the asymmetry of the instantaneous direction $\delta_e$, as shown in Fig. 4. The change of $\gamma_e$ has bulges in the second and third half-cycle, corresponding to the more intense radiated energy in Fig. 3. The directions of the electron motion and the radiations in the second half-cycle are the same as that in the fourth half-cycle. The two overlapped radiation pulses interfere with each other, producing the pattern shown in Fig. 3(d), where the minus value of the radiated energy in the fourth half-cycle indicates the energy is absorbed by the electron in the perspective of QED.

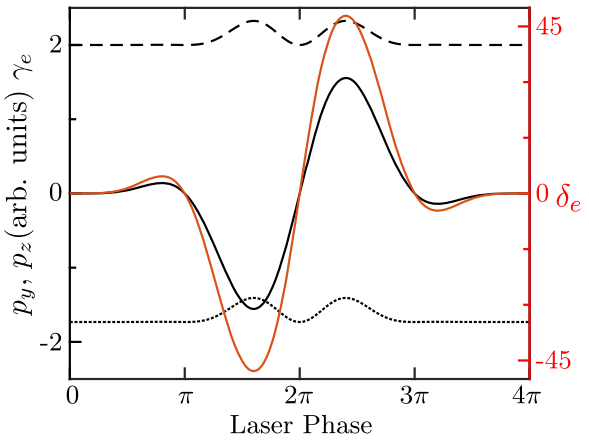


FIG. 4. The dependence of the $p_y$ (solid black curve), $p_z$ (dotted black curve), $\gamma_e$ (dashed black curve), and $\delta_e$ (solid red curve) on the laser pulse phase $\phi_L$.

### C. Results for oblique collision

Figure 5(a) shows the angular-distributed spectra of the radiation for the case of laser-electron oblique collision at $\theta = 135^o$. The laser CEP = 0. Figure 5(b) shows the corresponding kinetic properties of the electron in the frame of $\Sigma'$. The new frame $\Sigma'(x'y'z')$ in Fig. 1(b) is obtained after rotating the $yoz$ plane by 45° counterclockwise. The angular spectra of the radiation loses its symmetry with respect to the initial laser propagation direction $\theta = 135^o$. The rate of change of $\theta$ with respect to $\omega'$ when $\theta > 135^o$ is larger than that when $\theta < 135^o$. This phenomenon is caused by the faster change of electron motion direction $\theta_e$ during $\theta > 135^o$. When $\theta_e < 135^o$, $p_{y\max} = 1.78$, and when $\theta_e > 135^o$, $p_{y\min} = -1.25$. When taking $p_y = 1.7$ for $\theta < 138^o$, $p_y = -1.35$ for $\theta < 138^o$, and $\omega_0 = 2.03$ eV in Eq. (5), the analytical relation between $\theta$ and $\omega'$ is drawn as the dashed lines in Fig. 5(a) and coincides well with the numerical results.

The location angle of the radiation beam axle gradually moves from the larger side to the lower side of $\theta \sim 135^o$ when the CEP changes from $-\pi/2$ to $\pi/2$ as seen in Fig. 6. When the CEP varies from 0 to $-\pi/2$ or $\pi/2$, the harmonics gradually exhibit a discrete structure, with each order spectral line becoming more continuous. This is because

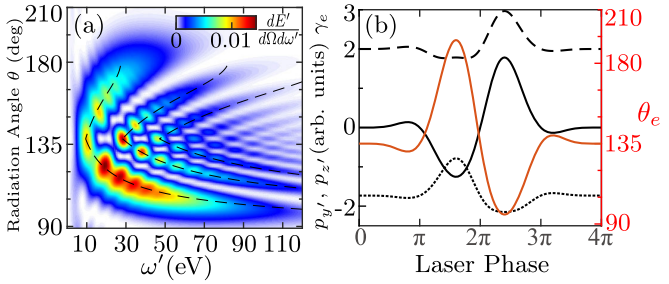


FIG. 5. (a) Angular-distributed spectra for laser-electron oblique collision with CEP = 0. (b) The dynamic parameters of the electron in the $\Sigma'$ frame $p_{y'}$ (solid black curve), $p_{z'}$ (dotted black curve), $\gamma_e$ (dashed black curve), and $\theta_e$ (solid red curve) as a function of laser phase.

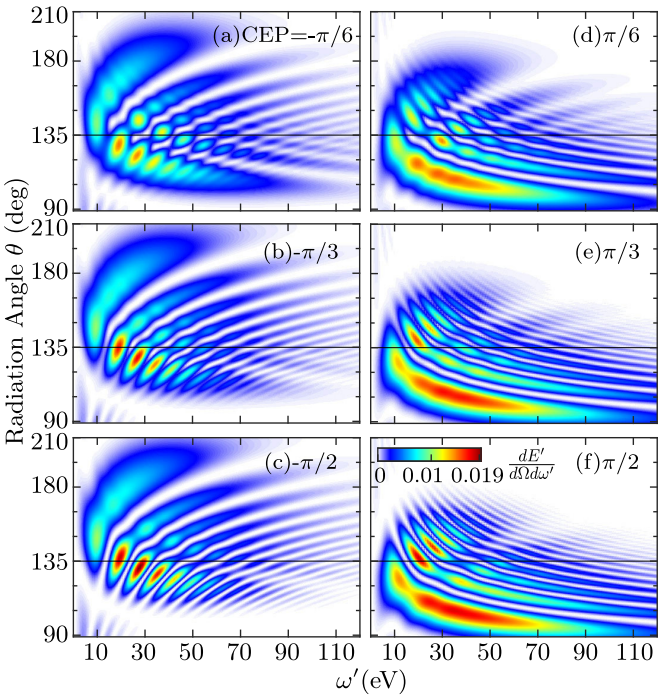


FIG. 6. Energy emission spectra for laser-electron oblique collision with different carrier envelope phases. All color bars are the same as in (f).

the electron motion direction $\theta_e$ has no overlap between $\theta_e > 135^o$ and $\theta_e < 135^o$ (see red line in Fig. 7) when $\phi_L \in [1.5\pi, 2.5\pi]$ and other phase ranges and thus the interference effect does not occur. The larger gamma factor during $\phi_L \in [0, 1.5\pi] \cup [2.5\pi, 4\pi]$ ($\phi_L \in [1.5\pi, 2.5\pi]$) corresponding to $\theta_e \in [115^o, 135^o]$ ($\theta_e \in [90^o, 135^o]$) for CEP $= -\pi/2$ and $\pi/2$ shown in Fig. 7 causes the different angular range of the more intense radiation energy distribution shown in Figs. 6(c) and 6(f).

Due to $\chi \ll 1$, the classical calculation results are similar to the quantum results as expected, and will be revisited when an electrostatic field is utilized as shown in Fig. 10. In Fig. 8, we set $\gamma = 2 \times 10^4$ and $\chi \sim 0.1$. There are obvious differences between quantum (red dotted line) and classical (blue line) results at higher emission frequencies. The quantum emission spectra have a divergent point at $\omega' = 10$ GeV, the energy of cutoff frequency $m\gamma$ as derived in the head-on collision case [18,23]. The classical calculation, however,

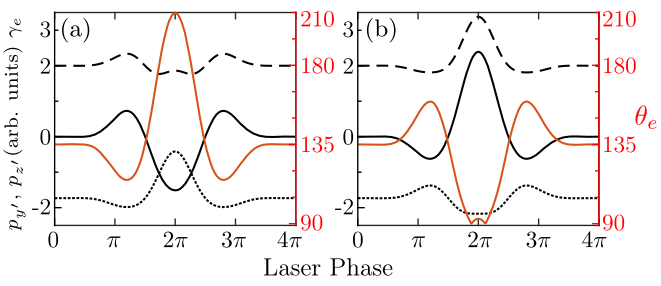


FIG. 7. The change of the dynamic parameters of the electron in the $\Sigma'$ frame for (a) CEP $= -\pi/2$ and (b) $\pi/2$. Each line has the same meaning as in Fig. 5(b).

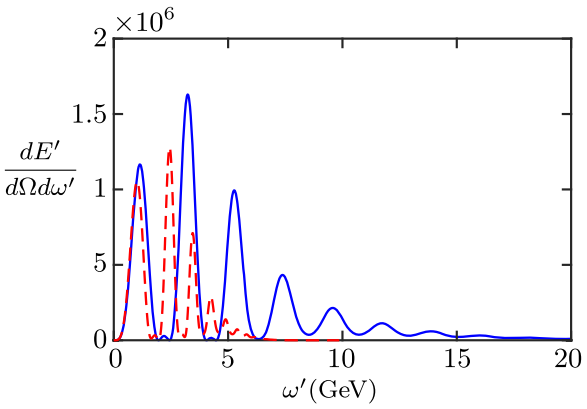


FIG. 8. Energy emission spectra for $\xi_L = 2$, CEP $= 0$, $\gamma = 10^4$, and emission angle $\theta = 135^o$. The red dotted line and blue line have been obtained from quantum and classical calculations, respectively.

gives nonphysical extension beyond the energy cutoff point, and decays slowly to the high-energy end.

## III. LASER-ELECTRON OBLIQUE COLLISION IN AN ELECTROSTATIC FIELD

### A. Description of the scenario

For an electron in both a laser field and an electrostatic field, we describe the electrostatic potential by a scalar potential, and its four-vector potential is described by $A_E^\mu = [-\psi_E(\phi_E)m\xi_E/e, 0, 0, 0]$, which do not satisfy the Lorentz gauge, causing $k_E A_E \neq 0$. In this case, the Dirac equation is written as $\gamma_\mu(i\partial^\mu - eA^\mu - m)\psi = 0$, where $A^\mu = A_L^\mu + A_E^\mu$, $A_L^\mu$ describes the laser field as above and $\gamma^\mu$ are the Dirac gamma matrices. The squared Dirac equation is derived as

$$[-\partial_\mu\partial^\mu - 2ieA^\mu\partial_\mu - ie(\partial_\mu A^\mu) + e^2A^2 - ie\not{k}_L\not{A}'_L - ie(\not{k}_E\not{A}'_E - k_E\not{A}'_E) - m^2]\psi = 0, \quad (9)$$

where the tag symbol means the derivative with respect to phase $\phi_L$ or $\phi_E$.

The solution is assumed to have the form $\psi = e^{-ipx}\mathcal{Z}(\phi_L, \phi_E)$. For the laser propagating in a diluted plasma as proposed in Ref. [33], the dispersion relations can be approximated to $(k_L)^2 \to 0$ and $(k_E)^2 \to 0$. Then, the above equation is reduced to

$$(2ik_Lp - 2iek_LA_E)\frac{\partial Z}{\partial\phi_L} + (2ik_Ep - 2iek_EA)\frac{\partial Z}{\partial\phi_E} + (-2eA_Lp + e^2A_L^2 - ie\not{k}_L\not{A}'_L - 2eA_Ep + e^2A_E^2 - ie\not{k}_E\not{A}'_E)Z = 0. \quad (10)$$

Using the method of variable separation, we set $Z = L(\phi_L)T(\phi_E)$ and transform the above equation into

$$\frac{\partial L}{\partial\phi_L}\frac{1}{L}(2ik_Lp - 2iek_LA_E) + I_1 = \lambda$$
$$\frac{\partial T}{\partial\phi_E}\frac{1}{T}(2ik_Ep - 2iek_EA) + I_2 = -\lambda \quad (11)$$

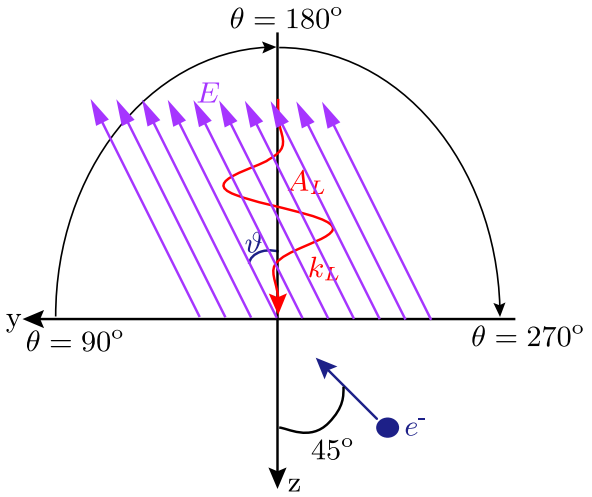


FIG. 9. Schematic illustration for laser-electron oblique collision within an electrostatic field.

with

$$I_1 = -2eA_L p + e^2 A_L^2 - ie\not{k}_L \not{A}'_L,$$
$$I_2 = -2eA_E p + e^2 A_E^2 - ie\not{k}_E \not{A}'_E,$$

where $\lambda$ is an arbitrary constant and can be taken as zero. Solving Eq. (11), we get the electron state as

$$\psi = \left(1 + \frac{e\not{k}_L \not{A}_L}{2(k_L p - ek_L A_E)}\right) \exp\left[\frac{e\not{k}_E \not{A}_E}{2(k_E p - ek_E A)}\right] \times \frac{u}{\sqrt{2p_0}} e^{iS(\phi_L, \phi_E)} \tag{12}$$

with

$$S(\phi_L, \phi_E) = -px - \int^{\phi_L} \frac{2eA_L p - e^2 A_L^2}{2k_L p - 2ek_L A_E} d\phi'_L - \int^{\phi_E} \frac{2eA_E p - e^2 A_E^2}{2k_E p - 2ek_E A} d\phi'_E. \tag{13}$$

Figure 9 shows the interaction scenario, and the electrostatic field has an angle $\vartheta$ to the negative laser direction. In order to facilitate the calculation of the integral in the scattering amplitude, the approximation $\phi_E \sim \phi_L$ is made for $\vartheta \leqslant 30°$, under which $\omega_E = \omega_L$. The range of $\phi_E$ is set to be the same as $\phi_L \in [0, 4\pi]$, otherwise $\psi_E(\phi_E) = 0$, which ensures that the electron is subjected to the electrostatic force while interacting with the laser pulse. The shape function $\psi_E(\phi_E) \approx -\phi_L$ and $k_E = (\omega_E, 0, -\omega_E \sin\vartheta, \omega_E \cos\vartheta)$.

We choose the small value of $\xi_E$ and $\vartheta$ to make the approximation that

$$k_L p - ek_L A_E \approx k_L p, \tag{14}$$

$$\exp\left[\frac{e\not{k}_E \not{A}_E}{2(k_E p - ek_E A)}\right] \approx 1 + \frac{e\not{k}_E \not{A}_E}{2k_E p}, \tag{15}$$

to further simplify the electron state Eq. (12) to

$$\psi = \left(1 + \frac{e\not{k}_L \not{A}_L}{2k_L p} + \frac{e\not{k}_E \not{A}_E}{2k_E p}\right) \frac{u}{\sqrt{2p_0}} e^{iS(\phi_L)}, \tag{16}$$

where the second-order term $e^2 \not{k}_L \not{A}_L \not{k}_E \not{A}_E / 4(k_L p)(k_E p)$ has been omitted.

The above electron state could be put into the calculation of the nonlinear single Compton scattering within an electrostatic field. The angular-frequency distribution of radiation can be expressed in the following form containing a tedious calculation of trace:

$$\frac{dE'}{d\Omega d\omega'} = \frac{e^2 \omega'^2}{8p^- p'^- (2\pi)^2} \mathrm{Tr}\left\{\sum_{\varepsilon'} [(\not{p}' + m)\mathcal{Z}(\not{p} + m)\overline{\mathcal{Z}}]\right\}, \tag{17}$$

where the bar operation on a matrix is defined as $\overline{\mathcal{Z}} = \gamma^0 \mathcal{Z}^\dagger \gamma^0$ with

$$\mathcal{Z} = \left(\frac{e\not{\varepsilon}'^* \not{k}_L \not{\phi}_L}{2k_L p} + \frac{e\not{\phi}_L \not{k}_L \not{\varepsilon}'^*}{2k_L p'}\right) f_{10} + \frac{-e^2 a_L^2 (k_L \varepsilon'^*) \not{k}_L}{2(k_L p)(k_L p')} f_{20} + \left(\frac{e\not{\varepsilon}'^* \not{k}_E \not{\phi}_E}{2k_E p} + \frac{e\not{\phi}_E \not{k}_E \not{\varepsilon}'^*}{2k_E p'}\right) f_{01} + \frac{e^2 (k_L \varepsilon'^*) \not{\phi}_E \not{k}_E \not{\phi}_E}{2(k_E p)(k_E p')} f_{02} + \left(\frac{e^2 \not{\phi}_L \not{k}_L \not{\varepsilon}'^* \not{k}_E \not{\phi}_E}{4(k_L p')(k_E p)} + \frac{e^2 \not{\phi}_E \not{k}_E \not{\varepsilon}'^* \not{k}_L \not{\phi}_L}{4(k_E p')(k_L p)}\right) f_{11} + \not{\varepsilon}'^* f_{00}, \tag{18}$$

where

$$f_{mn} = \int_0^{4\pi} \psi_L^m(\phi_L) \psi_E^n(\phi_L) e^{iS_1} d\phi_L, \tag{19}$$

with

$$S_1 = \xi \psi_L + \alpha \int_0^{\phi_L} \psi_L(\phi'_L) d\phi'_L + \beta \int_0^{\phi_L} \psi_L^2(\phi'_L) d\phi'_L + \kappa \int_0^{\phi_L} \psi_L(\phi'_L) d\phi'_L + \lambda \int_0^{\phi_L} \psi_L^2(\phi'_L) d\phi'_L, \tag{20}$$

where

$$\kappa = \frac{e(a_E p')}{k_E p'} - \frac{e(a_E p)}{k_E p}, \quad \lambda = \frac{e^2 a_E^2}{2k_E p} - \frac{e^2 a_E^2}{2k_E p'}. \tag{21}$$

The function $f_{00}$ can be written in the following form:

$$\xi f_{00} = -(\alpha f_{10} + \beta f_{20} + \kappa f_{01} + \lambda f_{02}). \tag{22}$$

### B. Numerical results

Figure 10 presents comparisons between the angular distribution of spectra calculated from quantum theory and classical theory, respectively. As shown in Figs. 10(a) and 10(b), the quantum results show obvious modulation effects of the static field on the angular spectra, whatever the CEP is, as compared to Fig. 6(f). In Fig. 10(b), when changing the direction of the static field, the energy spectra intensity is weakened and shifted to the low-energy end with the harmonic components becoming richer. In the calculation, the spectra is determined by the motion of the electron. The spectral modulation in Fig. 10(a) is due to the interference caused by the overlap of electron directions in different time intervals. Figures 10(c) and 10(d) are the results calculated from classical theory. In Fig. 10(c), the radiation spectrum moves slightly to low frequency compared to Fig. 6(f). When $\vartheta$ increases, as shown in Fig. 10(d), the radiation spectrum moves

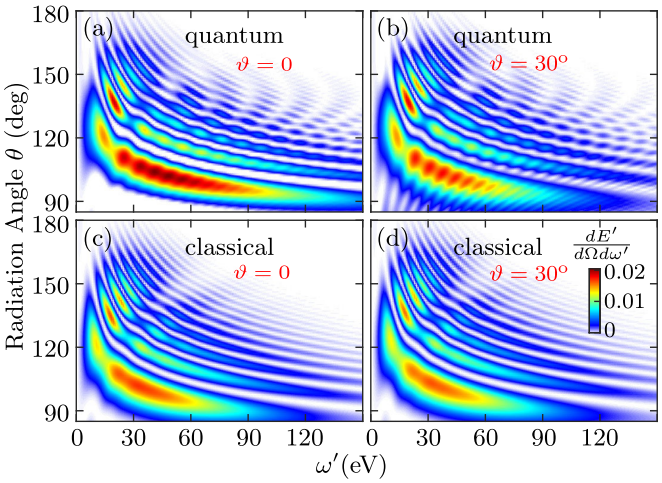


FIG. 10. Angular-distributed emission spectra for laser-electron oblique collision. The case is schemed in Fig. 9 with the direction of the electrostatic field having the angle $\vartheta = 0$ (left) and $\vartheta = 30^o$ (right) to the negative laser direction. (a) and (b) are the results from the quantum theory calculations, and (c) and (d) are those of classical theory calculations. In both calculations, CEP $= \pi/2$ and $\xi_E = 0.03$. Other parameters are the same as in Fig. 5(a). All color bars are the same as in (d).

to the lower-energy region compared to Fig. 10(c) because the electrostatic resistance increases. In both Figs. 10(c) and 10(d), the angular distributions of the radiation have a small change compared to that without electrostatic field due to the change of the electrostatic deflection force causing the change of electron motion direction.

## IV. SUMMARY

The NSCS process is investigated in the interaction of a multi-MeV electron with a two-cycle laser pulse of relativistic intensity in the framework of strong-field QED. For head-on and oblique collision, the improved analytical formula for the angular distribution of harmonic peaks agrees well with the results of the numerically resolved Dirac equation. For oblique collision, the peaks on the spectra become smoother due to the lack of interference among the emitted radiation from different time intervals of the laser pulse when the CEP-affected electron states have no large overlap in spatial distribution. This scenario is a simplified model of experiments about the high harmonic generation in relativistic laser-solid-target interaction. When the electrostatic field is utilized, it acts on the motion of the electron and thus affects the harmonic component and radiation angular distribution. The present study provides theoretical help in data analysis in attosecond-pulse-related strong laser field physic experiments.

## ACKNOWLEDGMENTS

This work is supported by the the National Natural Science Foundation of China (Grant No. 12034020), the Strategic Priority Research Program of Chinese Academy of Sciences (Grant No. XDA25030300), and the Science Foundation of Shandong Province (Grants No. ZR2019ZD44 and No. 2022HWYQ-073).

[1] N. Narozhny and M. Fofanov, J. Exp. Theor. Phys. **90**, 415 (2000).
[2] V. N. Nedoreshta, A. I. Voroshilo, and S. P. Roshchupkin, Phys. Rev. A **88**, 052109 (2013).
[3] T. N. Wistisen, Phys. Rev. D **90**, 125008 (2014).
[4] K. Krajewska and J. Z. Kamiński, Phys. Rev. A **90**, 052117 (2014).
[5] T. Erber, Rev. Mod. Phys. **38**, 626 (1966).
[6] C. Müller, A. B. Voitkiv, and N. Grün, Phys. Rev. A **67**, 063407 (2003).
[7] A. I. Titov, H. Takabe, B. Kämpfer, and A. Hosaka, Phys. Rev. Lett. **108**, 240406 (2012).
[8] B. King and H. Ruhl, Phys. Rev. D **88**, 013005 (2013).
[9] M. J. A. Jansen and C. Müller, Phys. Rev. A **88**, 052125 (2013).
[10] T. Nousch, D. Seipt, B. Kämpfer, and A. Titov, Phys. Lett. B **755**, 162 (2016).
[11] A. R. Bell and J. G. Kirk, Phys. Rev. Lett. **101**, 200403 (2008).
[12] S. Meuren, K. Z. Hatsagortsyan, C. H. Keitel, and A. Di Piazza, Phys. Rev. D **91**, 013009 (2015).
[13] A. Ilderton, P. Johansson, and M. Marklund, Phys. Rev. A **84**, 032119 (2011).
[14] J. Schwinger, Phys. Rev. **82**, 664 (1951).
[15] Y. Lau, F. He, D. P. Umstadter, and R. Kowalczyk, Phys. Plasmas **10**, 2155 (2003).
[16] M. Boca and V. Florescu, Eur. Phys. J. D **61**, 449 (2011).
[17] M. Boca and A. Oprea, Phys. Scr. **83**, 055404 (2011).
[18] D. Seipt and B. Kämpfer, Phys. Rev. A **83**, 022101 (2011).
[19] A. I. Nikishov and V. I. Ritus, Zh. Eksp. Teor. Fiz. **46**, 776 (1963) [Sov. Phys. JETP **19**, 529 (1964)].
[20] M. Boca and V. Florescu, Phys. Rev. A **80**, 053403 (2009).
[21] T. Heinzl, D. Seipt, and B. Kämpfer, Phys. Rev. A **81**, 022125 (2010).
[22] D. Seipt and B. Kämpfer, Laser Phys. **23**, 075301 (2013).
[23] F. Mackenroth and A. Di Piazza, Phys. Rev. A **83**, 032106 (2011).
[24] K. Krajewska and J. Z. Kamiński, Phys. Rev. A **85**, 062102 (2012).
[25] F. Mackenroth, A. Di Piazza, and C. H. Keitel, Phys. Rev. Lett. **105**, 063903 (2010).
[26] D. Seipt and B. Kämpfer, Phys. Rev. A **88**, 012127 (2013).
[27] D. M. Wolkow, Z. Phys. **94**, 250 (1935).
[28] V. B. Berestetskii, E. M. Lifshitz, and L. P. Pitaevskii, *Quantum Electrodynamics*, Vol. 4 (Butterworth-Heinemann, Oxford, 1982).
[29] A. Angioi, F. Mackenroth, and A. Di Piazza, Phys. Rev. A **93**, 052102 (2016).
[30] F. Mackenroth, N. Kumar, N. Neitz, and C. H. Keitel, Phys. Rev. E **99**, 033205 (2019).
[31] E. Raicher, S. Eliezer, and A. Zigler, Phys. Plasmas **21**, 053103 (2014).

[32] E. Raicher and S. Eliezer, Phys. Rev. A **88**, 022113 (2013).
[33] J. T. Mendonca and A. Serbeto, Phys. Rev. E **83**, 026406 (2011).
[34] E. Raicher, S. Eliezer, and A. Zigler, Phys. Lett. B **750**, 76 (2015).
[35] E. Raicher, S. Eliezer, and A. Zigler, Phys. Rev. A **94**, 062105 (2016).
[36] D. an der Brügge and A. Pukhov, Phys. Plasmas **17**, 033110 (2010).
[37] B. Dromey, S. Rykovanov, M. Yeung, R. Hörlein, D. Jung, D. Gautier, T. Dzelzainis, D. Kiefer, S. Palaniyppan, R. Shah *et al.*, Nat. Phys. **8**, 804 (2012).
[38] M. Yeung, B. Dromey, S. Cousens, T. Dzelzainis, D. Kiefer, J. Schreiber, J. H. Bin, W. Ma, C. Kreuzer, J. Meyer-ter-Vehn, M. J. V. Streeter, P. S. Foster, S. Rykovanov, and M. Zepf, Phys. Rev. Lett. **112**, 123902 (2014).
[39] S. Cousens, B. Reville, B. Dromey, and M. Zepf, Phys. Rev. Lett. **116**, 083901 (2016).
[40] W. Furry, Phys. Rev. **81**, 115 (1951).
[41] V. Ritus, J. Sov. Laser Res. **6**, 497 (1985).
[42] F. J. Dyson, Phys. Rev. **75**, 1736 (1949).
[43] A. Di Piazza, K. Z. Hatsagortsyan, and C. H. Keitel, Phys. Rev. Lett. **105**, 220403 (2010).
[44] J. Meyer-ter Vehn, A. Pukhov, and Zh.-M. Sheng, in *Atoms, Solids, and Plasmas in Super-Intense Laser Fields* (Springer, New York, 2001), pp. 167–192.
[45] J. Meyer-ter-Vehn and H.-C. Wu, Eur. Phys. J. D **55**, 433 (2009).